Design and fabrication of refractive nulls for testing the segmented mirrors of the Constellation-X spectroscopy x-ray telescope (SXT)

J. P. Lehan[*a], T. Hadjimichael[b], D. A. Content, and W. W. Zhang

NASA Goddard Space Flight Center, Greenbelt, Maryland 20771

[a]University Space Research Association, Suite 620, 10211 Wincopin Circle, Columbia, Maryland 21044
[b]Swales Aerospace, 5050 Powder Mill Road, Beltsville, Maryland 20705

ABSTRACT

We designed a refractive null lens for (visible) optical testing of the segmented mirrors for the Constellation-X spectroscopy x-ray telescope. We explored two solution families and identified the trade-offs. We also present some initial results of the realization of one solution family.

Keywords: Optical testing, lens design, Constellation-X, x-ray telescope, OAP

1. INTRODUCTION

The problems arising from testing grazing-incidence optics are now well known yet no general solution has been forthcoming. The primary issue comes from the foreshortening of the pupil. This results in the optical information being compressed along one dimension at best and shadowing of a fraction of the surface at worst. This is particularly bad in the case of x-ray optics where the incidence angles are of the order of 89º from the normal to assure total external reflection. To eliminate the foreshortening and accurately characterize the surface, we have opted to test the individual mirror segments for the Constellation-X Spectroscopy X-ray Telescope (SXT)[1] in normal incidence.

The telescope design is of segmented Wolter I construction consisting of hundreds of concentric reflector shells nested one inside another. This nested design is preferred from the standpoint of stacking in space. It is an attempt to try to regain telescope collection area lost by the grazing incidence foreshortening of the individual pupils without requiring a much larger spacecraft. This classic design consists of a reflection off a paraboloid of revolution (primary) followed by a second reflection from a hyperboloid of revolution (secondary) to a focus, which almost meets the Abbe sine condition. Several variations on this theme have arisen to either improve the field of view[2] or (slightly) ease fabrication.[3,4] For the Optical Alignment Pathfinder[5] (OAP) discussed here; we have adopted one of the latter approaches where the hyperboloid and paraboloid are replaced by a generalized toroidal surface. This lower-order approximation to their respective conic section has the property that the primary and secondary have equal curvature parallel to the optical axis.[4] For the long focal length of the OAP design (8.5 meters); this approximation has minimal effect on the image quality. It does, however, ease the testing task by increasing the symmetry of the parts under test.

Further, the segmentation of each nested shell eases the fabrication and testing tasks since the full 360º of the telescope is broken into pieces, making access to the inner surface of the telescope stages for normally-incident testing trivial. The problem remains, however, that each nested telescope and each stage has a unique prescription resulting in hundreds of different optical prescriptions to test to high precision. It is desirable to have a unified solution to the testing to manage the complexity and cost. We describe here one attempt to address these issues.

[*] e-mail: lehan@lheapop.gsfc.nasa.gov phone: (301) 286-0671

Optics for EUV, X-Ray, and Gamma-Ray Astronomy II, edited by Oberto Citterio, Stephen L. O'Dell,
Proc. of SPIE Vol. 5900, 59001D, (2005) · 0277-786X/05/$15 · doi: 10.1117/12.615316

2. SEGMENTED WOLTER I OPTICS TESTING

The lowest order approximation to the hyperboloid and paraboloid used in Wolter I telescopes is the cone. If a cone is tested in normal incidence, the cross-sections become ellipses, each cross section having the same eccentricity. The variation in radius of curvature as one moves parallel to the cone axis is accommodated by tilting the optic by the half-angle to obtain retrace. If we then take the next term in the expansion of the hyperboloid or paraboloid, we have what appears to be a "sagged cone" or a generalized toroid. The difference between the various axial cross sections (down the telescope barrel) and that of the corresponding conic section (hyperboloid) is shown in Fig. 1 to illustrate the magnitude of the error made in these approximations.

When the *sagged* cone is tested at normal incidence, the cross sections are no longer ellipses with the same eccentricity. If, however, the cone half-angle is small and axial length of interest not too long (true in our case), the change in eccentricity as one moves down the axis over the mirror is negligible.

Applying the same thinking outlined above for the cone to the sagged cone, the part can be thought of as equivalent to a sagged elliptical cylinder. To summarize, the conditions that bring this about are as follows: the large telescope F/# (~ 8.5 for the outermost telescope shell), $c_x >> c_y$, and the part is viewed normal to the surface (which results in the changing propagation distance parallel to the axis resulting from the cone half-angle tilt). This model is the basis for the null lens design scheme we discuss below.

The sagged elliptical cylinder is a specific case of the biconic surface. The equation for the biconic in this case is expressed as

$$z = \frac{c_x x^2 + c_y y^2}{1 + \sqrt{1 - (1 + k_x) c_x^2 x^2 - c_y^2 y^2}}, \quad (1)$$

where c_x and c_y are base curvatures along the azimuthal (x) and axial (y) directions, and k_x is the conic constant in the azimuthal direction (the conic constant in the axial direction is zero).

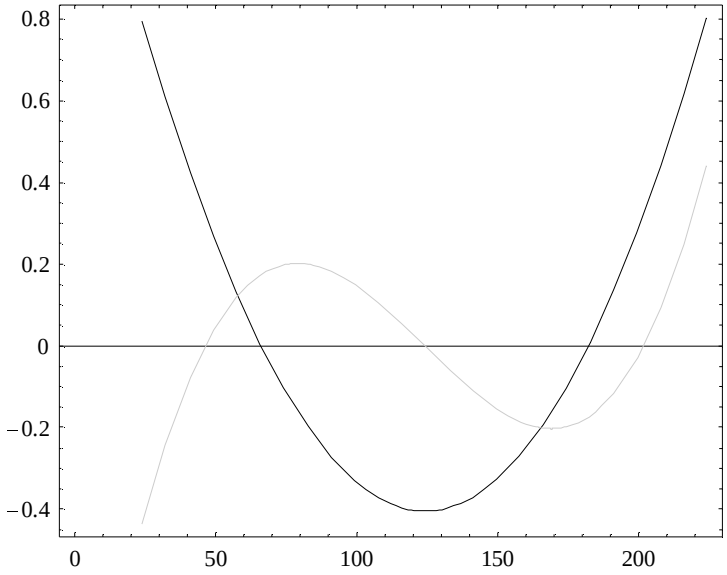

Figure 1: Difference between the conical and second-order approximations versus the exact hyperboloid for a Wolter I telescope secondary. The horizontal scale is mm and the vertical scale is microns. The black line (—) is the conical approximation with ~0.12 micron P-V deviation from the hyperboloid. The gray line (—) is the 2nd order approximation (multiplied by 100) with a P-V deviation of ~ 8 nm. [The telescope secondary for this example has a mid-point azimuthal radius of curvature of 244.4 mm and the telescope focal length is 8.5 meters. The conic constant for the hyperboloid is -1.000433. We will use this reflector as the example for our subsequent analysis.]

3. NULL LENS DESIGN

The null lens consists of two parts, the first is a well-corrected cylindrical lens, and the second is a hybrid element with different surface types on each face. The cylindrical part is common to all the mirror shells under test whereas the hybrid

element varies from shell to shell. Such an approach reduces the number of elements that need to be manufactured and tested since the cylindrical portion may be recycled as the shell testing proceeds.

The assumed geometry is shown in Fig. 2. A collimated beam from our Fizeau interferometer passes through the null lens, is reflected off the part, and passes back through the null lens and into the interferometer.

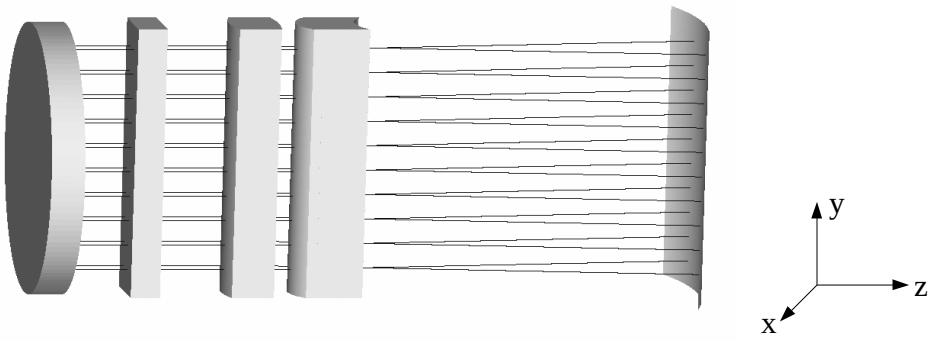

Figure 2: Geometry assumed in the design problem. The reference flat of the Fizeau interferometer is shown at the far left. The three elements of the null lens (from left to right – hybrid element, cylindrical singlet, cylindrical cemented doublet) are shown in the center and the reflector under test at the right. The system is double-pass through the null lens group.

A. Cylindrical lens design

We considered a large number of design options. The effective azimuthal F/# of one segment is 0.93, independent of telescope shell. Although we can design an air spaced lens for this fast a system, the number of surfaces and alignment tolerances were unlikely to be met. This is particularly true given the 210 mm axial length of the lenses. Instead, we opted for an F/1.5 design that has only three elements, two of which are cemented together. This greatly reduces the optomechanical alignment task since only two elements need be aligned, but requires us to stitch two interferograms to yield a full surface map for each segment. The stitching, however, is purely azimuthal (in x only) so that any stitching errors have little impact on the determination of the smaller curvature (c_y), which is most influential in the telescope performance.

To improve manufacturability, only preferred glasses were allowed. We designed the lenses using the Zemax optical design program. The resulting design is shown in Fig. 3. To aid convergence and improve design stability, we optimized the design at two different closely spaced laser wavelengths (632.8 and 638.0 nm) although the lens only needs to function at one (632.8 nm). We found that this trick greatly reduced the number of local minima that the lens design program found and, we believe, resulted in a more manufacturable design. Final optimization, however, was performed only at the wavelength of intended use.

The optical design program does not have tolerancing tools for non-rotationally symmetric systems so we wrote our own scripts to perform the tolerancing. As expected, the non-powered axis residual power (usually called irregularity), alignment of the surface axes, and axis skew were found to be the most sensitive errors.

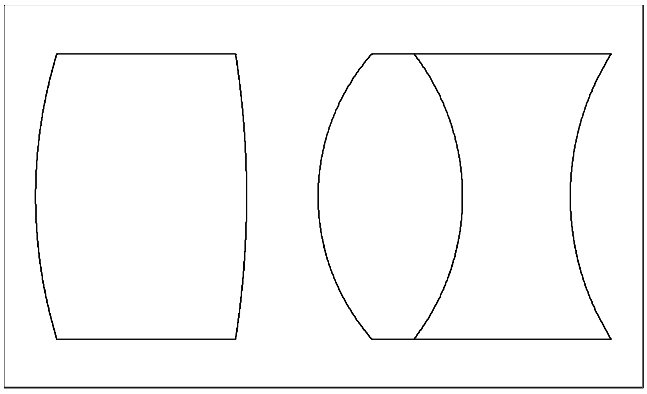

Surface	Radius (mm)	Thickness (mm)	Glass
S1	86.08796	37	S-BAL35
S2	-163.2278	12.54391	Air
S3	37.93861	25.32528	S-BAL14
S4	-41.04251	18.88794	S-NPH2
S5	47.28007		

Figure3: The cylindrical lens portion of null lens. This design was chosen due to greater ease of assembly than some of the other alternatives are.

B. Acylindrical corrector design

The design of the hybrid element is unique since this element produces the departure from a cylinder for each primary or secondary reflector. There are two families of solutions. The first family has the shell corrector element prior to the cylindrical lens assembly whereas the second family has the hybrid element serving as a field lens. The two solution families have different advantages. With the hybrid element in front of the cylindrical lens assembly, the alignment task is quite simple and so swapping it from shell to shell to measure the different reflector designs is straightforward. The disadvantages are that the sags of the surfaces are so small as to be difficult to accurately determine and thus manufacture. With the hybrid element in the field lens position, the performance is essentially unchanged and the sags of the surfaces are more manufacturable, but the positioning of the element is less simple. We discuss both solutions for a particular reflector design below.

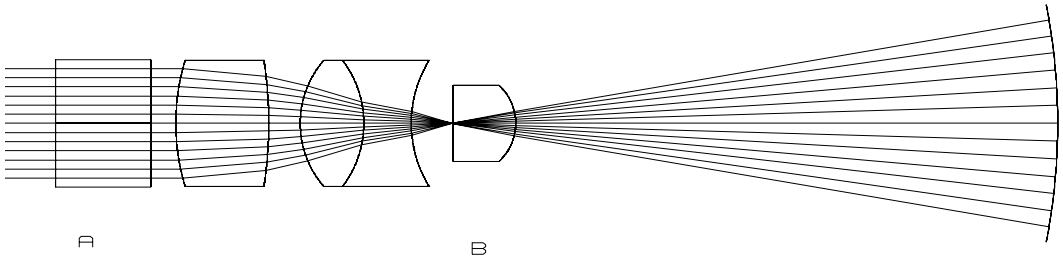

Figure 4: Test set-up viewed from above indicating the two solution families. The hybrid element for family one is shown in position A above, the hybrid element for family two is shown at position B. (Note: Only one hybrid element is required for any test and the two in the figure above is merely illustrative of the approximate shapes and positions relative to the cylindrical triplet.)

The prescription for the hybrid element for solution family one is given in Table I. Note that neither surface has much power and the element essentially imparts an aberration to the plane wave entering the cylindrical lens. This element could be split into two if the alignment of the center of the spherical surface and cylindrical axis proves too problematic to produce.

Surface	Radius (m)	Thickness (mm)	Glass	Surface Type
S1	79.9106	33	Fused Silica	Cylinder
S2	2080.59		Air	Sphere

Table I: Prescription for one of the hybrid elements for testing the second order approximation to the secondary hyperboloid (see also Fig. 1 caption for more description of the surface). The axis for this element is perpendicular to that of the cylinders of Fig. 3.

The RMS error for this corrector used in conjunction with the cylindrical lens of Fig. 3 is less than $1/50^{th}$ wave RMS in the double-pass null test. Of note is that the errors are almost entirely azimuthal (x) and the axial (y) errors are negligible. Thus, this design is quite acceptable since the azimuthal errors in the reflectors under test are less critical than the axial errors for telescope performance.

The prescription for the hybrid element for solution family two is given in Table II. This surface consists of two crossed cylindrical surfaces.

Surface	Radius (m)	Thickness (mm)	Glass	Surface Type
S1	-2098.3	25	Fused Silica	Cylinder
S2	-0.0204		Air	Cylinder

Table II: Prescription for one of the hybrid elements for testing the same reflector as in Table I but in the field lens position. The axis for the first element is perpendicular to the axis of the cylinder lens group of Fig. 3. The second axis is parallel to them.

The RMS error for this corrector, in conjunction with the cylindrical lens of Fig. 3, is also about $1/50^{th}$ wave RMS in the double-pass null test. In this case, the errors are acceptably small in both the azimuthal (x) and the axial (y) directions. The illuminated area of the part, however, is reduced azimuthally.

The operation of the field lens corrector can be thought of as follows: The first cylindrical surface of the field lens corrector imparts the needed curvature of the wavefront axially (x). The second surface adds a small amount of aberration in the azimuthal direction (y). This approximates the required acylindrical departure of the wavefront azimuthally.

4. MOUNTING AND INITIAL PERFORMANCE RESULTS

Optimax Systems, Inc. fabricated the lenses. The manufacturing process is limited by the surface metrology, which, in turn, is limited by the 95 mm diameter of the Diffraction International CGH (H95F3C). Full surface maps were stitched together using our stitching program described briefly elsewhere[6] and augmented by axial scans.

Given the system is for use in a laboratory setting, the requirements on the optomechanical design are less stringent in terms of durability. There are no precision commercial mounts of this size and the standard texts on optomechanical design do not address the precision mounting of cylindrical lenses either. For laboratory work, we decided to mount the lenses between two plates held together with four precision shafts. The plates are co-drilled to assure alignment of the shafts and avoid skewing of the plates. The lenses are contacted at the top and bottom by three Delrin balls to minimize localized high-stress points in the lenses, although the lenses are oversized in this dimension so that any mounting stress will have a minimum impact on the transmitted wavefront in the clear aperture of the lens. The plate assemblies are mounted to a New Focus five-axis positioner that allows us sufficient degrees of freedom to align the lenses for minimum wavefront error. Figure 6 shows the lens as mounted.

As of this writing, several elements are still awaiting fabrication including the hybrid element. We present an initial comparison between predicted performance from surface measurements and measured transmitted wavefront. Figure 7 shows the axial wavefront as measured and predicted from the stitched surface maps. The test beam for the transmission measurement is less than 190 mm diameter with only an 178 mm clear aperture (wavefront better than $1/20^{th}$ wave P-V). As a result, we could not test the entire 210 mm of the axial clear aperture of the lens. The agreement

between the two methods is excellent over the clear aperture of the test beam and deviates at one end where the test beam is known to deviate from planarity. The residual tilt between the components of the test results in an uncertainty in the registration of this deviation making the correction of it less certain. This result yields independent verification of the accuracy of the stitched interferograms. We note also that the residual wavefront curvature is within the tolerance for given for this element.

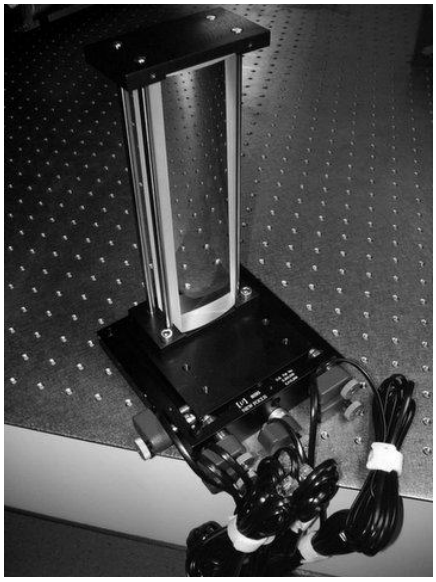

Figure 6: Cylindrical singlet mounted for alignment to cylindrical doublet illustrating mounting and alignment schemes. The four rods are precision ground and positioned outside the clear aperture of the lens. The lens rests on three plastic balls in a machined recess so that only a few mm^2 are lost. The cylindrical doublet is mounted behind the singlet shown and the five-axis stage used to co-align them.

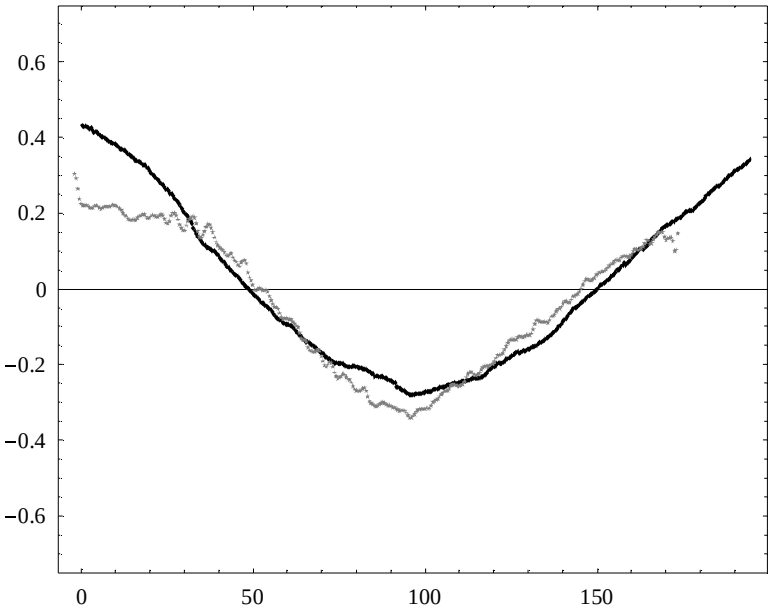

Figure 7: Comparison between the axial transmitted wavefront determined from the stitched interferograms of surfaces S1 and S2 (——) and measured in transmission (···). The vertical units are waves (single pass) and the horizontal scale is mm. The residual error on the left hand side is due to the inability to correct for the residual wavefront error in the undersized test beam (see discussion).

5. SUMMARY

We described the design methodology employed to obtain a refractive null lens for testing the mirrors for the Constellation-X SXT. The advantage of the method is that it is based upon a common core with only one element changing as one tests each unique reflector design. In addition, all the surfaces are either spherical or cylindrical and so are more cost-effectively manufactured than aspheric or acylindrical surfaces.

We identified and discussed two families of solution. The two families were concerned with the unique element that is changed to match a specific mirror shell. It was found that both families gave adequate performance.

ACKNOWLEDGEMENTS

We would like to thank NASA for supporting this work through the Constellation-X mission program. We also wish to acknowledge helpful discussions with Dr. Timo Saha, and Dr. Robert Petre. We would also like to thank Mr. Rick Plympton, Mr. Allan Gould and Mr. Joe Serio of Optimax Systems, Inc. for providing the interferograms for the performance prediction.

REFERENCES

1) R. Petre, D. A. Content, J. P. Lehan, S. L. O'Dell, S. M. Owens, W. A. Podgorski, J. Stewart, and W. W. Zhang, "The Constellation-X Spectroscopy X-ray Telescope," *Proc. SPIE* **5488**, 505, (2004).

2) J. E. Harvey, A. Krywonos, P. L. Thompson, and T. T. Saha, "Grazing-incidence hyperboloid-hyperboloid designs for wide-field x-ray imaging applications," *Applied Optics*, **40**, 136 (2001).

3) R. Petre, and P. J. Serlemitsos, "Conical imaging mirrors for high-speed x-ray telescopes," *Applied Optics*, **24**, 1833 (1985).

4) T. T. Saha, and W. Zhang, "Equal-Curvature Grazing-Incidence X-Ray Telescopes," *Applied Optics*, **42**, 4599 (2003).

5) J. H. Hair, J. W. Stewart, R. Petre, W. W. Zhang, D. A. Content, T. T. Saha, W. A. Podgorski, P. E. Glenn, M. L. Schattenburg, R. K. Heilmann, Y. Sun, and G. Nanan, "Constellation-X spectroscopy x-ray telescope segmented optic assembly and alignment implementation," *Proc. SPIE* **4851**, 696 (2003).

6) D. A. Content, D. Colella, C. Fleetwood, T. Hadjimichael, J. P. Lehan, J. McMann, P. Reid, T. Saha, G. Wright, and W. Zhang, "Optical metrology for the segmented optics on the Constellation-X Spectroscopy X-ray telescope," *Proc. SPIE*, **5488**, 272 (2004).